Geophys. J. Int. (1996) **127**, 215–229

Induced stresses and fault potential in eastern Canada due to a realistic load: a preliminary analysis

Patrick Wu[1] and Henry S. Hasegawa[2]

[1]*Department of Geology & Geophysics, University of Calgary, Calgary, AB, Canada,* T2N-1N4

[2]4936 *Brodys Place, Nanaimo, BC, Canada,* V9T-5Y3

Accepted 1996 June 6. Received 1996 May 2; in original form 1995 December 20

SUMMARY

In order to understand the causal relation between postglacial rebound and earthquakes, a realistic ice and water load model is used to (1) calculate stresses induced in the lithosphere and mantle by glacial loading, melting and postglacial rebound and (2) evaluate the effect of glacial loading/rebound on the failure potential for earthquakes in the upper crust. The dependence of both the failure potential and the actual mode of failure on the ambient tectonic stress magnitude, the overburden stress, and lithospheric properties are investigated. Prominent features of this analysis are the inclusion of (1) a viscoelastic mantle and thus the migration of stress, and (2) the ambient tectonic stress and overburden stress contributions in the calculation of the total stress field.

The spatio–temporal calculations, by a finite-element technique, of upper-crustal stresses and the failure potential for earthquakes indicate that fault stability is invariably enhanced directly beneath the load. For the case where stresses induced by the overburden are such that the horizontal component (S_h) is greater than or equal to the vertical component (S_v) ($\zeta \geq 1$, where $\zeta = S_h/S_v$), the model predicts the onset of thrust faulting and maximum earthquake activities soon after deglaciation is complete (when rebound rates are at a maximum). Observational data support this prediction. Since that time, rebound stresses have been decreasing in magnitude, but they continue to act as a trigger mechanism for optimally oriented pre-existing faults that are otherwise on the verge of failure. If one limits the existence of such faults to lie within the pre-weakened zones of eastern Canada, then the spatial distribution of current earthquakes can also be explained.

Perturbations to the magnitude of the tectonic stress components or lithospheric properties do not affect, to any significant extent, the above conclusions.

Key words: earthquakes, faulting, postglacial rebound, seismicity, stress.

1 INTRODUCTION

Although eastern Canada is in an intraplate (mid-plate) seismotectonic environment, it experiences large earthquakes with magnitudes as high as *M*7. The distribution of recent earthquakes in eastern Canada with magnitude greater than *M*3 is plotted in Fig. 1(a), which shows that most of the seismic activity is along the following three tectonic trends: (1) the Baffin Bay–Grand Banks portion of the Mesozoic rifted margin that lies offshore of eastern Canada; (2) the reactivated Palaeozoic structures along the Boothia Uplift–Bell Arch; and (3) the Palaeozoic rifts along the St. Lawrence Valley–Ottawa Bonnechere Graben (Adams & Basham 1989).

The focal mechanisms of the larger events indicate that thrust faulting is dominant in eastern Canada. However, there are exceptions to this general trend: along the northeast coast of Baffin Island, focal mechanisms of the larger earthquakes are of the normal-fault type. In contrast, in the northeastern United States, strike-slip faulting predominates (Herrmann 1979; Hasegawa, Adams & Yamazaki 1985; Talwani & Rajendran 1991; Zoback 1992). Interspersed are regions where thrust faulting has been documented (Herrmann 1979; Nabelek & Suarez 1989).

There is evidence that eastern Canada has been seismically active since early postglacial times. This is indicated by the presence of postglacial thrust faults (Adams 1989, 1996) and earthquake-related mud slumping (Shilts, Rappol & Blais 1992) in southeastern Canada. An important question that emerges from studies of these earthquakes is 'what role does postglacial rebound stress play in current seismic and faulting

Earthquake location and magnitude

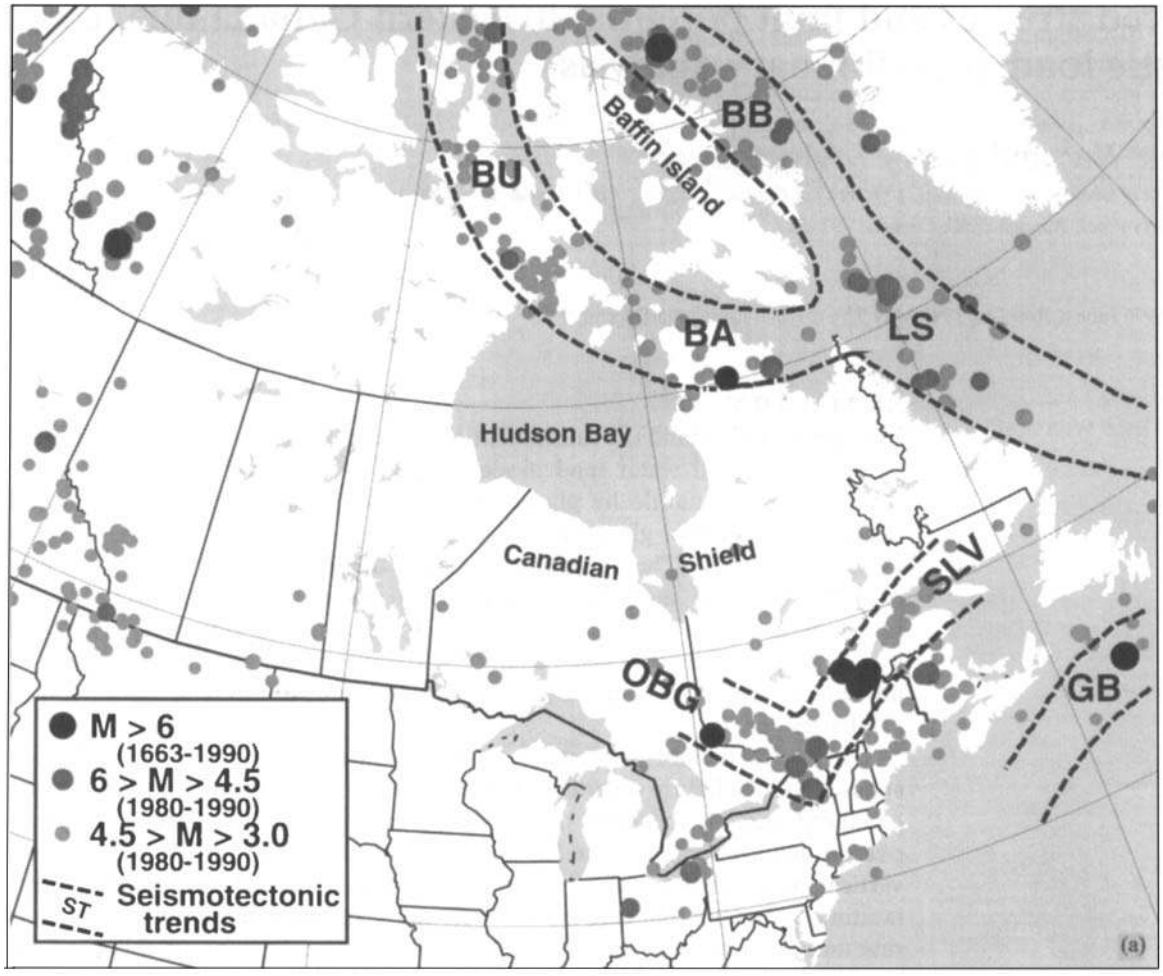

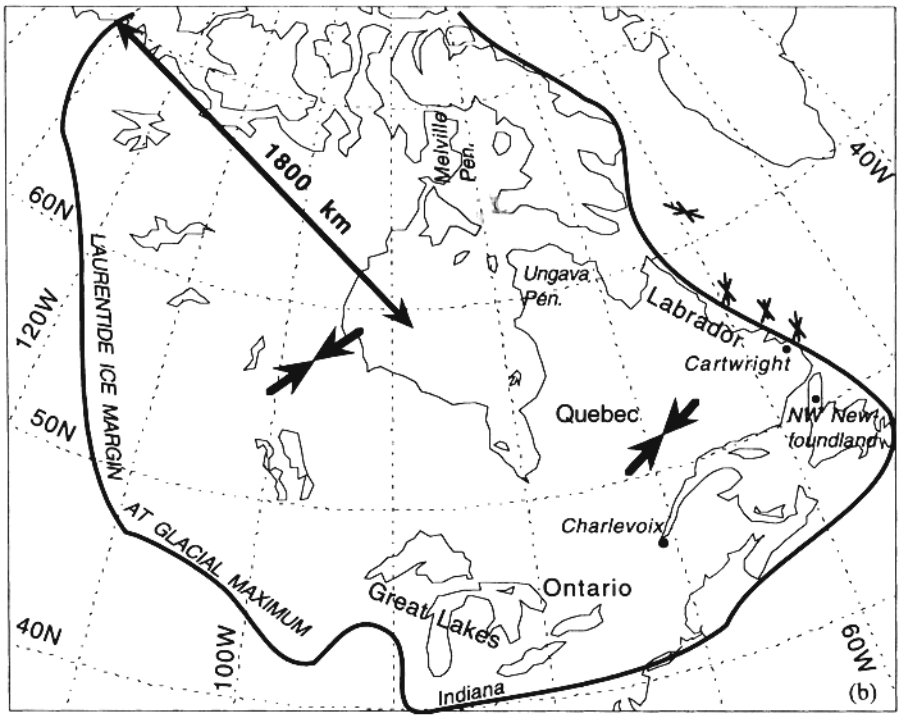

activity in eastern Canada?' This is a relevant question because at the last glacial maximum 18–19 Ka BP (thousand years before present), the Laurentide ice sheet covered most of Canada and parts of the northeastern United States (Fig. 2), with an average ice thickness of about 2500 m (or vertical stress of about 25 MPa) and flexural stresses exceeding 50 MPa. This expansive ice sheet, however, deglaciated rapidly around 12–10 Ka BP, and melting was almost complete by about 8 Ka BP. Thus, depending on the rate of relaxation, rebound-induced stresses have the potential to trigger seismic and faulting activity in eastern Canada.

Analysis of the correlation between glacial phenomena (glacial loading, melting and postglacial rebound) and stresses induced in the lithosphere started with simple (*ad hoc*) models of ice loads and earth structure. Using a 2-D model of an ice sheet superimposed on an elastic lithosphere overlying an inviscid mantle (thus neglecting the important effects of stress relaxation), Walcott (1970) calculated the rebound stress pattern in the lithosphere near the edge of the ice sheet. Using a comparable ice load and earth model, but based on the premise that the neutral stress state in the lithosphere is with the ice load on, Stein *et al.* (1979) concluded that rebound stresses, *per se*, can actually dictate the mode of failure of earthquakes: normal faulting along the northeast coast of Baffin Island and thrust faulting under the contiguous Baffin Bay. However, this basic premise of Stein *et al.* (1979), when applied to earthquake activity in southeastern Canada and in the contiguous northeastern United States, predicts a sense of faulting that is not in agreement with what is actually observed (Hasegawa *et al.* 1985; Talwani & Rajendran 1991; Zoback 1992). Quinlan (1984), who considers rebound stress as a perturbation of an ambient tectonic stress field, states that rebound stresses, *per se*, can rarely dictate the actual mode of failure (in northeastern Canada) but can act as a trigger mechanism for faults that are otherwise close to failure. In addition to postglacial rebound, Hasegawa & Adams (1990) stated that pronounced topography (the mountain range along the northeast coast of Baffin Island) and the transition from continental to oceanic crust are also major contributors to the seismotectonic environment (normal-fault regime) along the northeast coast of Baffin Island. Basham, Forsyth & Wetmiller (1977) and Hasegawa & Basham (1989) pointed out that steep gradients in postglacial-rebound contours correlate with bands of intense seismic activity. Johnston (1987, 1989) presented causative factors for the suppression of seismic activity under the Laurentide, Antarctica and Greenland ice sheets. Using a viscoelastic earth model in conjunction with a complicated disc load model, James & Bent (1994) calculated rebound strain rates in southeastern

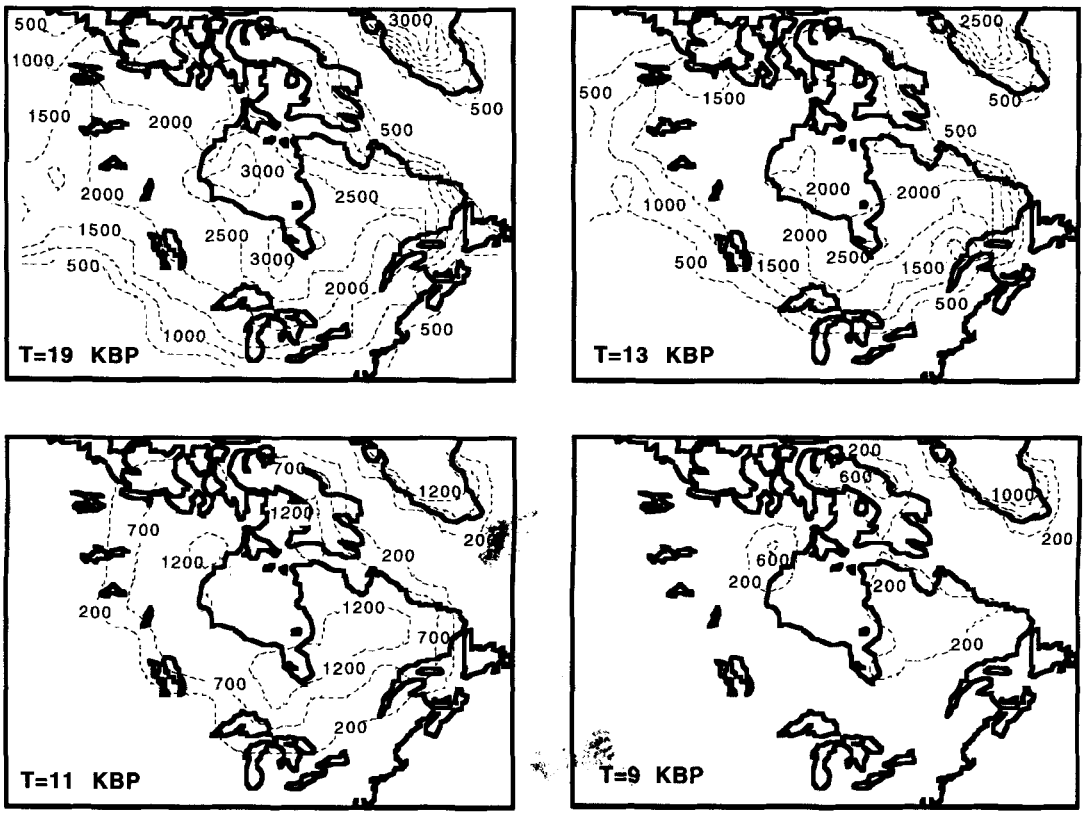

Figure 2. Adopted version of the ICE3G deglaciation history used to calculate a realistic spatio–temporal pattern of rebound and associated stresses. Contours are ice thickness in metres.

Figure 1. (a) Map of eastern Canada showing seismotectonic trends and earthquakes greater than $M3$ over specified time periods. Symbols are defined as follows. BU: Boothia Uplift; BA: Bell Arch; BB: Baffin Bay; LS: Labrador Sea; GB: Grand Banks; SLV: St. Lawrence Valley; OBG: Ottawa Bonnechere Graben (after Adams & Basham 1989). (b) Map of eastern Canada showing (1) the margin of the Laurentian ice-sheet during the glacial maximum (18 000 a BP), (2) the orientation of the contemporary stress field in eastern Canada, and (3) the location of some of the sites discussed in Figs 4, 6, 8, 10 and 12.

Canada and the northeastern United States. A comparison with seismic strain rates in the Charlevoix region of the St. Lawrence Valley indicated their rebound strain rates to be one to two orders of magnitude greater than seismic strain rates. Thus, in general, previous analyses of stresses, strains and earthquake activity due mainly to postglacial rebound stresses have been confined to localized regions of eastern Canada and the contiguous United States.

As a follow-up to these site-specific papers, Wu & Hasegawa (1996) (hereafter referred to as the companion paper) analysed

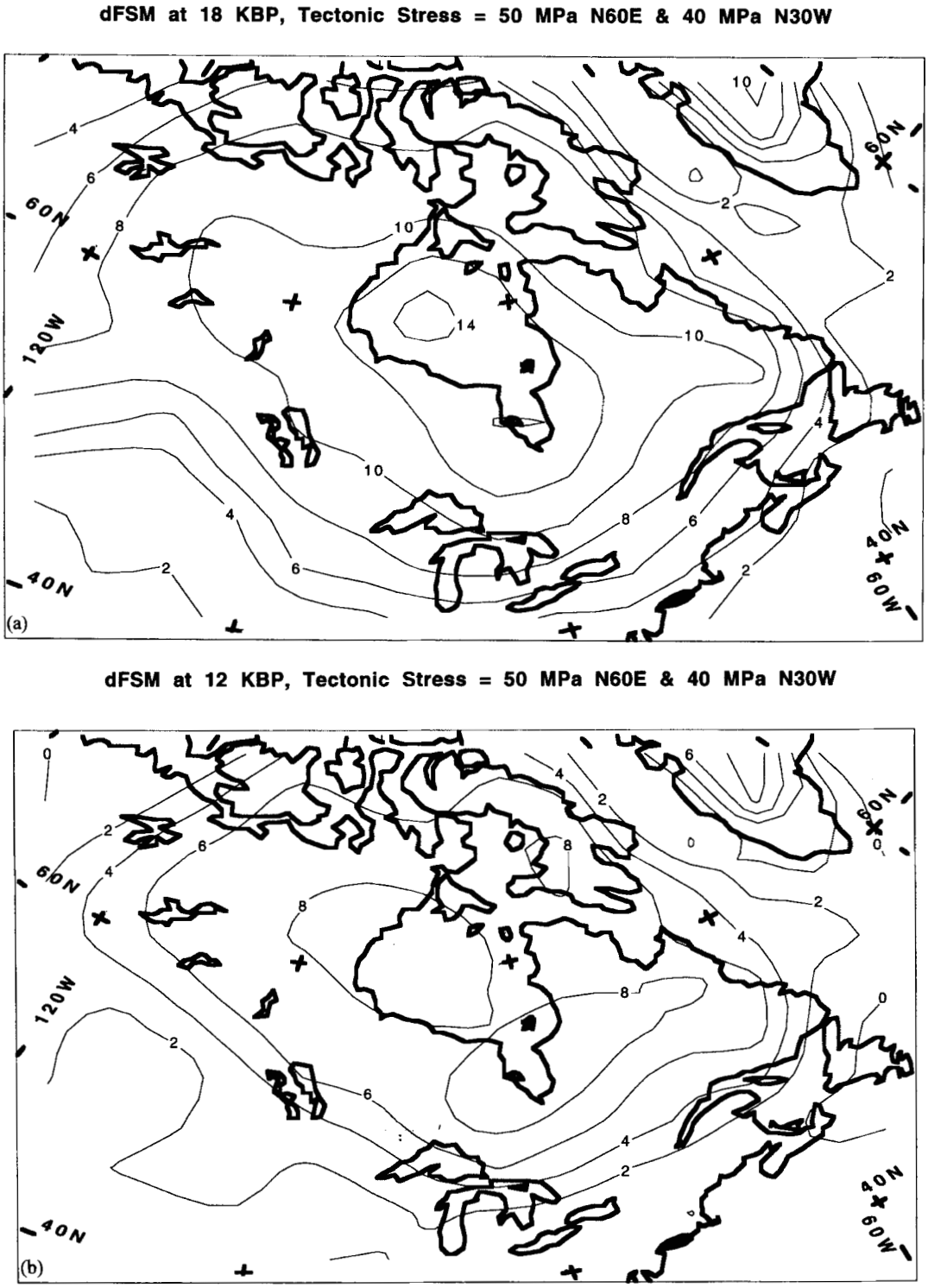

Figure 3. Spatio–temporal variation of dFSM in eastern Canada and the peripheral area, shown at four time periods at a seismogenic depth of 12.5 km. The total stresses used in the calculation include rebound stress, tectonic stress and overburden pressure, with $\zeta = 1$. The maximum tectonic principal stress is horizontal, oriented N60°E, and has a magnitude of 50 MPa, while that in the orthogonal direction is 40 MPa. A 200 km thick lithosphere has been used in the calculation. Contours are in MPa.

the spatio–temporal pattern of the induced stress over the entire area covered by the Laurentide ice sheet. In this simplified analysis, which was intended to outline general trends and not specific details, the mantle was taken to be viscoelastic and the ice sheet was simulated with a disc load having a Heaviside load–melt history. Moreover, the contributions of the ambient tectonic stress, overburden stress and rebound stress were all included in the calculation of failure potential. The main conclusions of Wu & Hasegawa (1996) were as follows.

(1) Crustal loading promotes fault stability directly underneath the load.

(2) Upon the removal of the load, thrust faulting is predicted

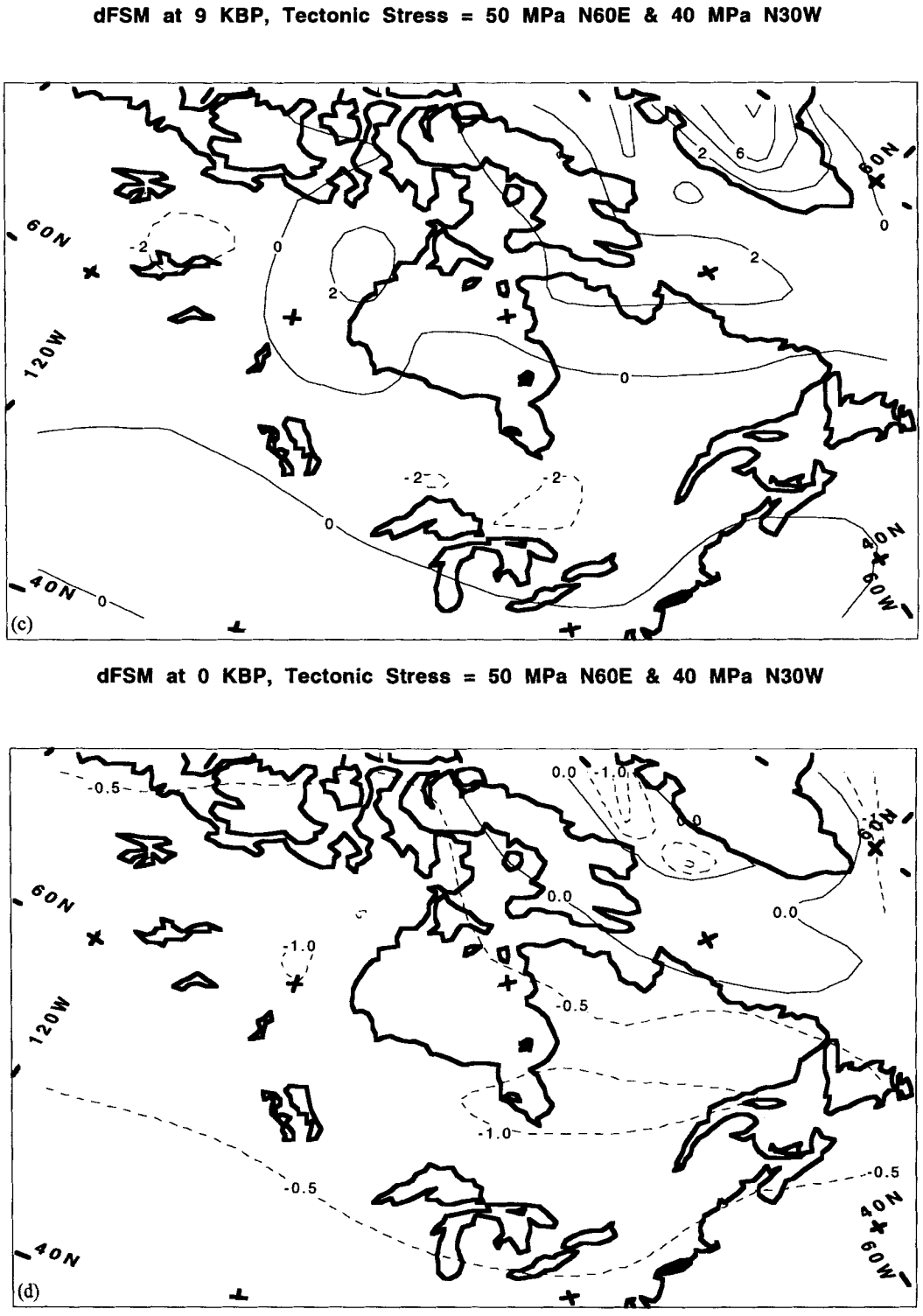

Figure 3. *(Continued.)*

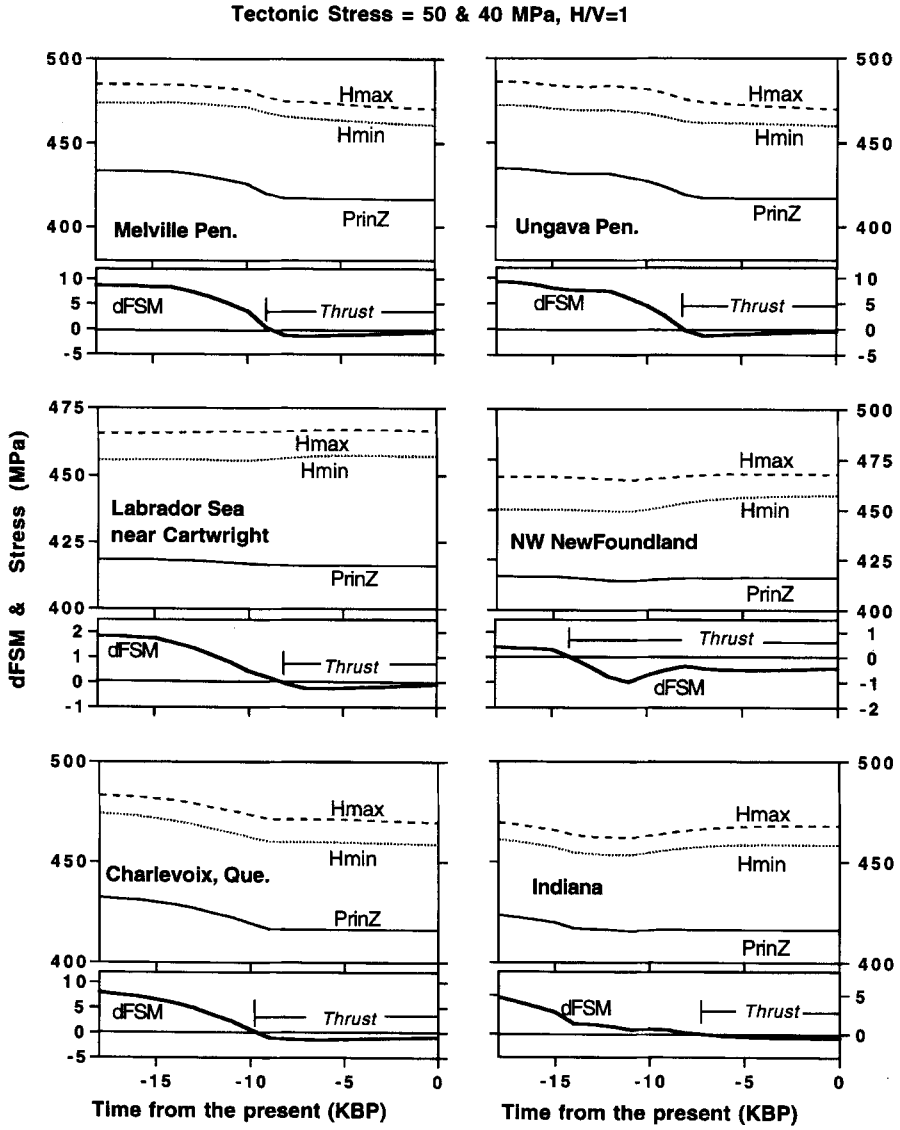

Figure 4. Evolution of the horizontal principal stresses (Hmax, Hmin), the vertical principal stress (PrinZ), dFSM and the mode of failure for the five sites shown in Fig. 1(b) and one (Indiana) in the northern US, all at a seismogenic depth of 12.5 km. The total stresses used in the calculation include rebound stress, tectonic stress and overburden pressure, with $\zeta = 1$. The maximum tectonic principal stress is oriented N60°E with a magnitude of 50 MPa, while that of the orthogonal component is 40 MPa. A 200 km thick lithosphere is used in the calculations.

within the ice margin if the overburden stress ratio, ζ (i.e. S_h/S_v, where S_v is the vertical overburden stress and S_h is the horizontal stress in the absence of tectonic and rebound stress components), is greater than or close to unity—in which case, fault stability within the ice margin should attain maximum instability immediately after deglaciation.

(3) If the value of ζ were small, then fault stability is predicted within the ice margin even after deglaciation.

(4) Fault instability is promoted both north and south of the ice load. The mode of failure, however, is completely determined by the value of ζ: thrust faulting for values close to or greater than unity; strike-slip for values just smaller than unity; and normal faulting for even smaller values of ζ.

In the present study, the disc load in the companion paper is replaced by a realistic model, namely the Tushingham & Peltier (1991, 1992) ICE3-G model, and the loading of the sea floor by the melted ice water is also included. As in the companion paper, the objectives are to: (1) calculate stresses induced in the lithosphere and mantle by glacial loading, melting and postglacial rebound; (2) evaluate the effect of glacial loading/rebound on the failure potential for earthquakes and the mode of failure in the upper crust; and (3) study the effect of ambient tectonic stress magnitude, overburden stress and lithospheric properties on failure potential and the mode of failure.

Like the companion paper, prominent features of this paper are the inclusion of: (1) a viscoelastic mantle and thus the migration of stress; and (2) the ambient tectonic stress and overburden stress contributions in the calculation of the total stress field.

As in the companion paper, a time-dependent quantity

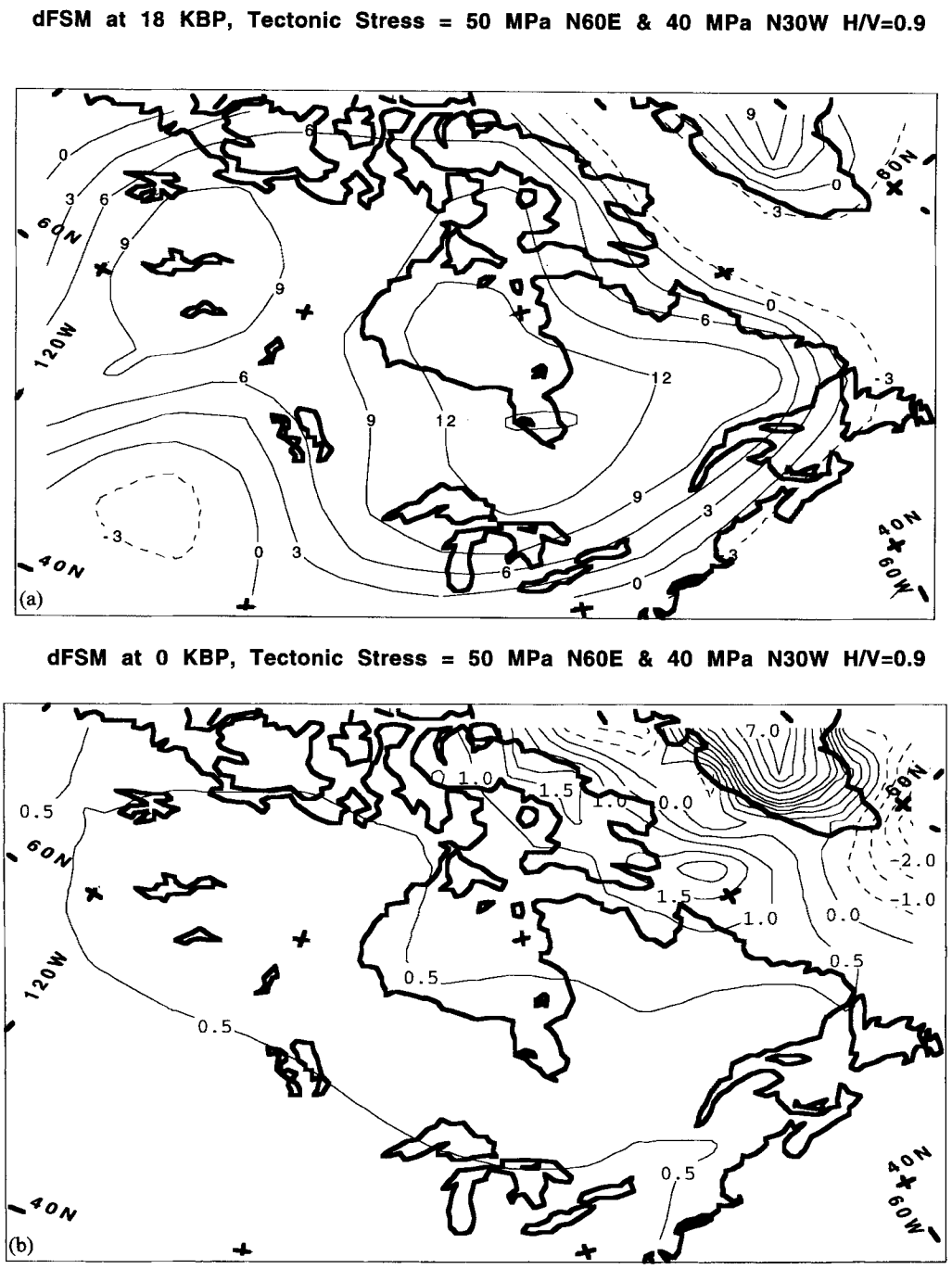

Figure 5. Similar to Fig. 3, except that the overburden stress ratio $\zeta=0.9$. (a) is for $t=18$ Ka BP and (b) is for $t=0$ Ka BP.

called dFSM can be defined:

$$dFSM(t)=\tfrac{1}{2}\{[\sigma_1(t_0)-\sigma_3(t_0)]-[\sigma_1(t)-\sigma_3(t)]\} + \mu\beta\{[\sigma_1(t)+\sigma_3(t)]-[\sigma_1(t_0)+\sigma_3(t_0)]\}, \quad (1)$$

where

$$\beta=\sin[\arctan(\mu)]/2\mu, \quad (2)$$

and μ is the coefficient of friction, taken to be 0.6, t is the time under consideration, t_0 is the time before the onset of glaciation, and σ_1, σ_2 and σ_3 are the maximum, intermediate and minimum (compressive) principal stresses, respectively. If, as is assumed, throughout the Earth there are optimally oriented pre-existing virtual faults that are initially close to, but not at, failure, then a negative value of dFSM would mean an enhanced likelihood of faulting, whereas a positive value of dFSM indicates that fault stability is enhanced.

In the next section, the model and the computational procedure of this study are described. Next, the results of a realistic ice- and ocean-loading history are discussed. Finally, the results of this paper are summarized.

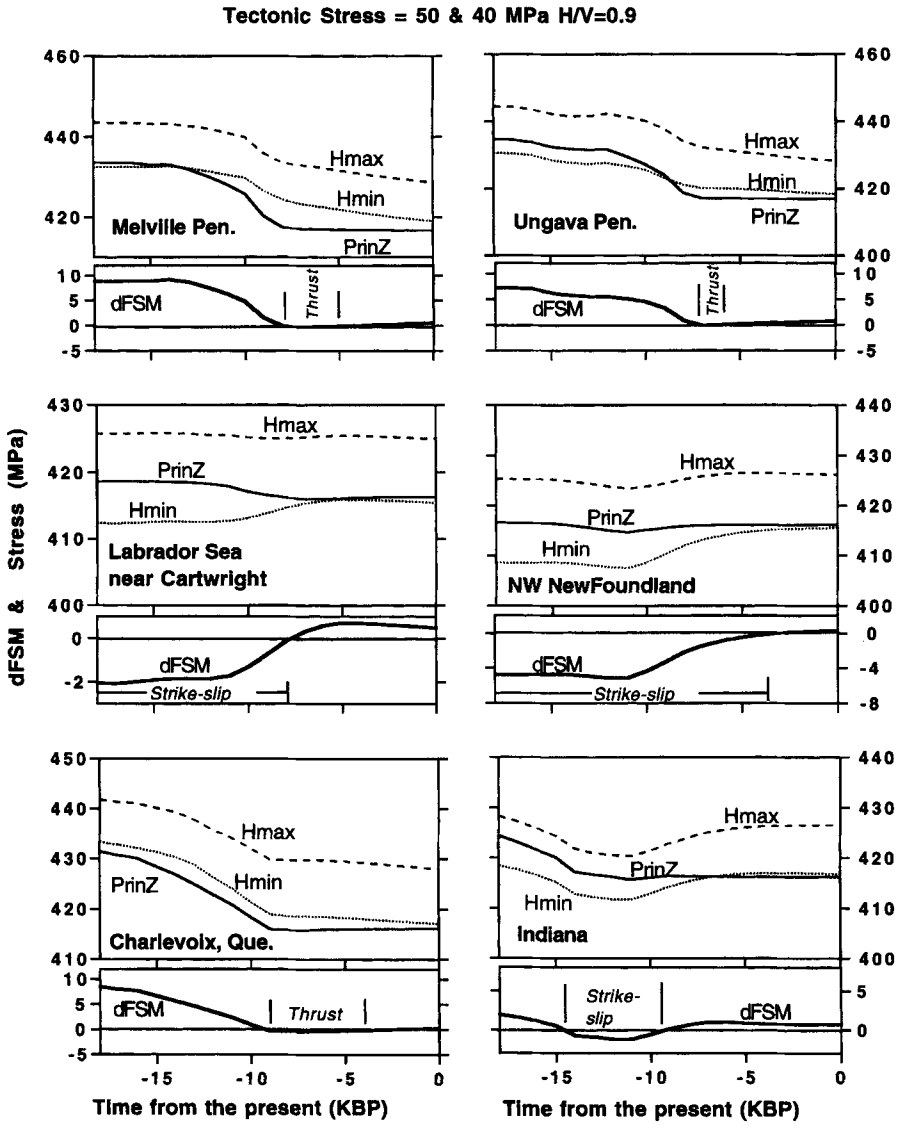

Figure 6. Similar to Fig. 4, except that the overburden stress ratio $\zeta = 0.9$.

2 MODELLING REBOUND STRESSES

Postglacial rebound has been successfully modelled using the finite element (FE) package ABAQUS (Wu 1992, 1993); the same technique is applied in this paper.

As in the companion paper, the momentum equation to be solved is given by:

$$\nabla \cdot \boldsymbol{\sigma} - \rho g \nabla w = 0 \tag{3}$$

(Cathles 1975, eq. III-3), where $\boldsymbol{\sigma}$ is the rebound stress tensor, w is the vertical component of the displacement $\mathbf{u}$, ρ is the density and g is the gravitational acceleration. The solution of this equation consists of the three components of the displacement, $\mathbf{u}$, and the six components of the rebound stress tensor, $\boldsymbol{\sigma}$, at every grid point in space and time. When eq. (3) is solved, $\boldsymbol{\sigma}$ contains contributions from the advected pre-stress ($\rho g w$), which acts as a pressure term. However, the advected pre-stress varies as a function of time (since w changes), and consequently must be included in the computation of dFSM (see companion paper).

There are two sets of data input to this FE program: an earth model and a load model. The earth model considered here is a compressible, stratified, flat earth that consists of an elastic lithosphere on top of isotropic, viscoelastic Maxwell layers in the mantle that, in turn, overlie an inviscid fluid core. The flat-earth approximation has been shown to be acceptable even for loads as extensive as the Laurentide ice-sheet (Amelung & Wolf 1994). The viscosity of the mantle is taken to be 1×10^{21} Pa s. The companion paper has demonstrated that lithospheric thickness does not affect dFSM or the mode of failure. The effects of mantle viscosity are discussed in Wu (1996). The initial state of the Earth is assumed to be deglaciated (certainly true before the onset of the Pleistocene glaciation) and without any bending stresses—only tectonic stress and overburden exist in the initial state.

Stress induced by the ice/water load is computed with the ABAQUS FE program on a Fujitsu VPX240 supercomputer. The earth model is composed of 10 layers with each layer consisting of 34×32 eight-node 3-D solid elements and 128 eight-node 3-D boundary elements. The area of active loading

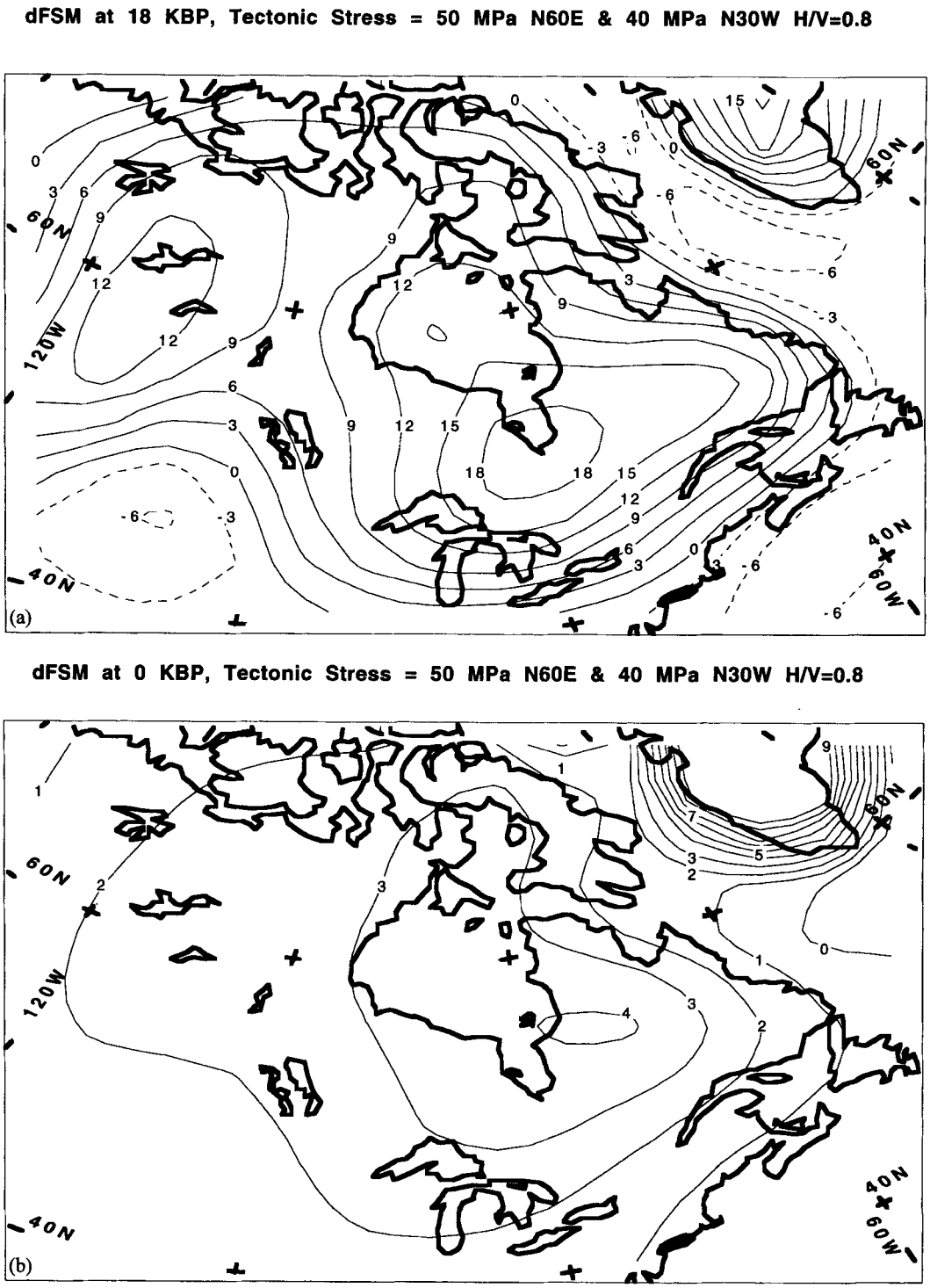

Figure 7. Similar to Fig. 3, except that the overburden stress ratio $\zeta = 0.8$. (a) is for $t = 18$ Ka BP and (b) is for $t = 0$ Ka BP.

is covered by 16×14 active elements which lie in the centre at the top of the $34 \times 32 \times 10$ solid elements. Each of these active elements has horizontal dimensions of 340 km $\times$ 323 km. The maps in this paper (i.e. Figs 3, 5, 7 and 9) only show the 14×12 active elements over eastern Canada. The other elements that surround the active elements are not actively loaded and their dimensions increase as they approach the boundary elements. Such gridding is used to mimic the infinite extent of each layer.

In this paper, the deglaciation of the Laurentian, Cordillera, Innuition and Greenland ice-sheets described in the ICE3G model of Tushingham & Peltier (1991, 1992) is adopted. Since ICE3G gives an uneven ice grid on a spherical surface, the grid is first projected (using Lambert equal-area projection) onto a flat surface, and the ice thicknesses are then interpolated onto the regular 16×14 active grid. The adopted deglaciation history is shown in Fig. 2, where contours of the ice thickness (in metres) at four discrete times are plotted. It should be

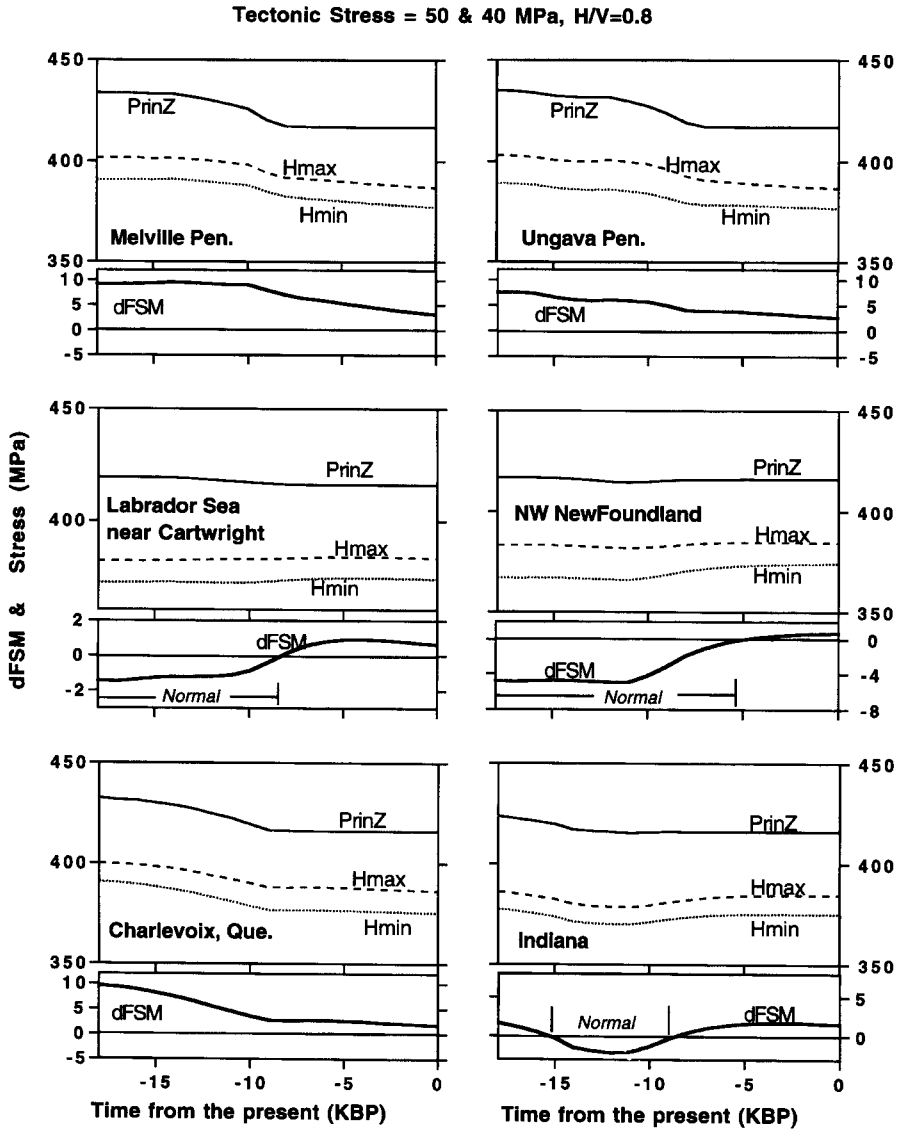

Figure 8. Similar to Fig. 4, except that the overburden stress ratio $\zeta = 0.8$.

noted that ICE3G only gives the deglacial part of the ice history during the last 18 000 years. To include the effect of the previous glacial cycles, recall that oxygen isotope data from deep-sea cores indicate that during the last 2–3 Myr glacial build-up has been very slow (on the order of 100 000 years), whereas deglaciation has been much faster (on the order of 10 000 years). Thus the ice thickness at every location is assumed to follow the saw-tooth ice history described in Wu & Peltier (1982) before the last glacial maximum at 18 Ka BP.

Loading of the ocean by the melted ice water can be obtained by solving the gravitationally self-consistent sea-level equation (Farrell & Clark 1976; Peltier, Farrell & Clark 1978; Wu & Peltier 1983; Mitrovica & Peltier 1991). For the purpose of this paper, only the first-order approximation of the sea-level equation is solved, i.e. only the eustatic sea-level rise, the effects of unloading within the ice sheet and loading of the ocean floor are considered. For special places like Hudson Bay, the model takes into account the melting of the ice that transformed ice loads into water loads and the subsequent draining of Hudson Bay due to land uplift.

2.1 Computational procedure

In order to evaluate the effects of glacial loading/rebound on variations in the failure potential (dFSM) and the mode of failure for earthquakes, ambient tectonic stress and overburden stress components are also included. As explained in the companion paper, tectonic stress, overburden stress and pore fluid pressure are assumed to be time-independent, in which case pore fluid pressure can be neglected.

The total stress is obtained by summing tensorally the rebound stresses, the tectonic stresses and the overburden pressure at 12.5 km. The orientation of the tectonic maximum horizontal principal stress is taken to be in the N60°E direction (Adams 1989; Adams & Bell 1991; Zoback 1992). Due to the uncertainty in the magnitude of the tectonic principal stresses and the overburden stress parameter ζ, a range of values will be considered. The principal stresses are obtained by diagonalizing the total stress tensor. Changes in the fault stability margin (dFSM) are computed from eqs (1) and (2) with $\mu = 0.6$. Finally, the predicted temporal and spatial distributions

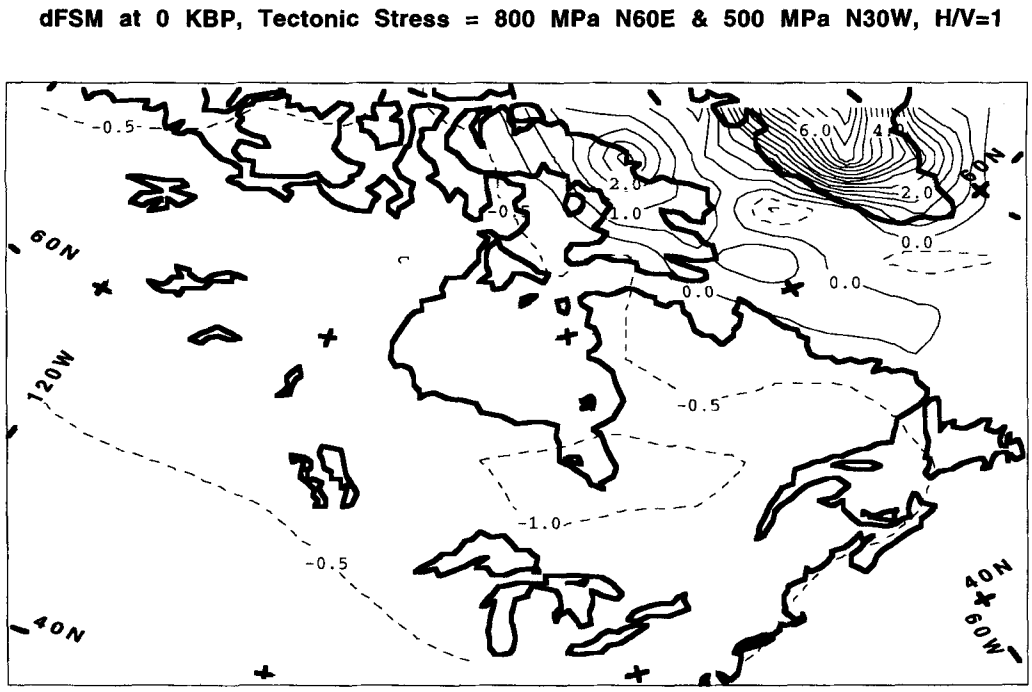

Figure 9. Similar to Fig. 3, except that the maximum tectonic principal stress has a magnitude of 800 MPa while that in the orthogonal direction is 500 MPa.

of dFSM and their modes of failure can be obtained (see companion paper).

3 RESULTS

3.1 Effect of the overburden parameter ζ

The value of ζ determines the rate at which the horizontal stress components increase with depth relative to the vertical component ($\zeta = S_h/S_v$). For the deglaciated state, the vertical stress is the minimum principal stress at the surface, so large values of ζ ($\geqslant 1$) will result in a thrust regime. With decreasing values of ζ, the regime changes to strike-slip and finally to normal faulting. As demonstrated in the companion paper, representative values of these three regimes at a depth of 12.5 km are $\zeta = 1$, 0.9 and 0.8 respectively; furthermore, these values remain approximately valid even under the ice load. So, in the following, we continue to use these three values to investigate the effect of overburden stress.

First, consider the case when $\zeta = 1$. For illustrative purposes, the maximum tectonic principal stress along N60°E is set at 50 MPa and the minimum tectonic principal stress at 40 MPa. Contour plots of dFSM at four time steps are shown in Fig. 3. At the glacial maximum, around 18 Ka BP, Fig. 3(a) shows that dFSM is strongly positive under the ice load (especially under Hudson Bay), but decreases beyond the ice margin. At 12 Ka BP, when the ice load is about one-half the maximum thickness, Fig. 3(b) shows that dFSM is still positive inside the ice margin, although the amplitude is much smaller. At 9 Ka BP, when there are only three pockets of ice remaining (Fig. 2), Fig. 3(c) shows that dFSM remains positive mainly under these pockets of ice. All these are consistent with the results of the disc load (see companion paper), which showed that fault stability is always promoted underneath the load, and for the peripheral zone outside the load, stability is also promoted for some time after loading. Around 9 Ka BP (Fig. 3c), dFSM becomes negative in the deglaciated areas in eastern Canada. A small positive ridge is also formed outside the ice margin south of the Great Lakes—this is approximately the location of the peripheral bulge. At present (0 Ka BP), there is a residual negative dFSM, on the order of 0.5–1.0 MPa, that extends to areas well beyond the ice margin at the glacial maximum (Fig. 3d). This is significant because stresses at this level can trigger earthquakes, as shown by induced seismicity studies and investigations of triggered seismicity following the Landers earthquake. Comparing Figs 3(c) and (d) shows that the amplitudes of the negative troughs show a decrease during the last 9000 years. These results confirm the findings of the disc-load model (companion paper), which predict fault instability in the deglaciated area and minimum dFSM (or maximum instability) soon after deglaciation.

The evolution of dFSM shown in Fig. 3 is presented for certain fixed locations in Fig. 4. In addition, the evolution of the total stress (expressed in terms of horizontal principal stresses Hmax, Hmin and the vertical principal stress PrinZ) and the modes of failure for five sites in eastern Canada and one in the northern US are also shown. The location of the sites can be found in Fig. 1(b). Inspection of Fig. 4 shows that for the sites along the Boothia Uplift–Bell Arch (Melville Pen. and Ungava Pen.), the Labrador coast and along the St. Lawrence Valley–Ottawa Bonnechere Graben (Charlevoix), dFSM becomes negative around 9–10 Ka BP and reaches a minimum value around 9–7 Ka BP. For pre-existing virtual faults that are optimally oriented and are initially close to failure before the onset of glaciation, this implies that earthquakes would begin around 10 Ka BP and reached maximum activity around 9–7 Ka BP. The mode of failure is predicted to be thrusting, which agrees with available data

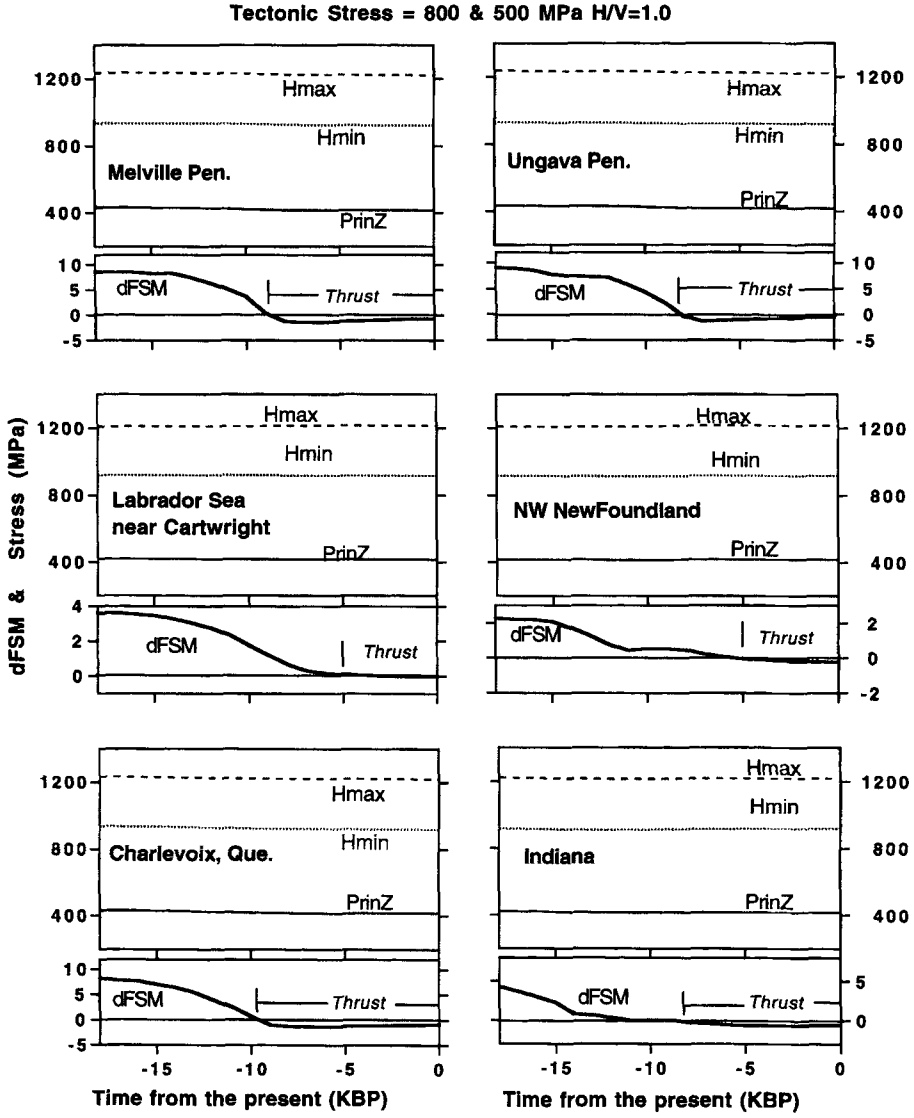

Figure 10. Similar to Fig. 4, except that the maximum tectonic principal stress has a magnitude of 800 MPa while that in the orthogonal direction is 500 MPa.

(Adams 1989). In Newfoundland, where melting is early, the mode of failure is again predicted to be thrust faulting but seismic activity is predicted to have begun much earlier, at around 14 Ka BP. At or beyond the ice margin in the northern United States (e.g. Indiana), seismic and faulting activity is predicted to have occurred later, at around 7 Ka BP, but the mode of failure is again predicted to be thrust faulting. Examples of pure thrust-fault earthquakes are the M_w5.4 southern Illinois earthquake of 1968 (Herrmann 1979) and the m_b5.1 Goodnow earthquake in New York State (Nabelek & Suarez 1989). Moreover, in Fig. 4 the prediction that dFSM would go negative at Indiana about 7–8 Ka BP coincides with the time frame of a very large (M_w7.5) Wabash Valley earthquake discovered and dated by palaeoliquefaction research (Obermeier *et al.* 1991), which adds credibility to the analysis.

Next, consider the case when $\zeta=0.9$ while the tectonic stresses remain as before. Fig. 5 shows the spatial distribution of dFSM at $t=18$ and 0 Ka BP while the evolution of the total stress, dFSM and mode of failure are shown in Fig. 6. Inspection of these figures shows that, as before, stability is promoted beneath the ice load. However, there are some significant differences: (1) during the loading phase, instability can be found near and beyond the edge of the ice sheet (e.g. the Labrador Sea near Cartwright, NW Newfoundland and Indiana), where the mode of failure is strike-slip; (2) immediately after load removal, deglaciated areas become unstable with either thrust or strike-slip faulting; however, this fault instability only lasts for a short duration; (3) at present, fault stability is predicted everywhere in eastern Canada and the peripheral area. These results are basically the same as those predicted by the disc model (companion paper), provided differences in the ice profile and the migration of the ice boundary are taken into account.

The results for $\zeta=0.8$ are shown in Figs 7 and 8. A comparison with Figs 5 and 6 shows that the effects are similar except that (1) the value of dFSM becomes more positive (especially after deglaciation): as a consequence, instability does not generally occur after deglaciation and fault stability is predicted everywhere in eastern Canada and

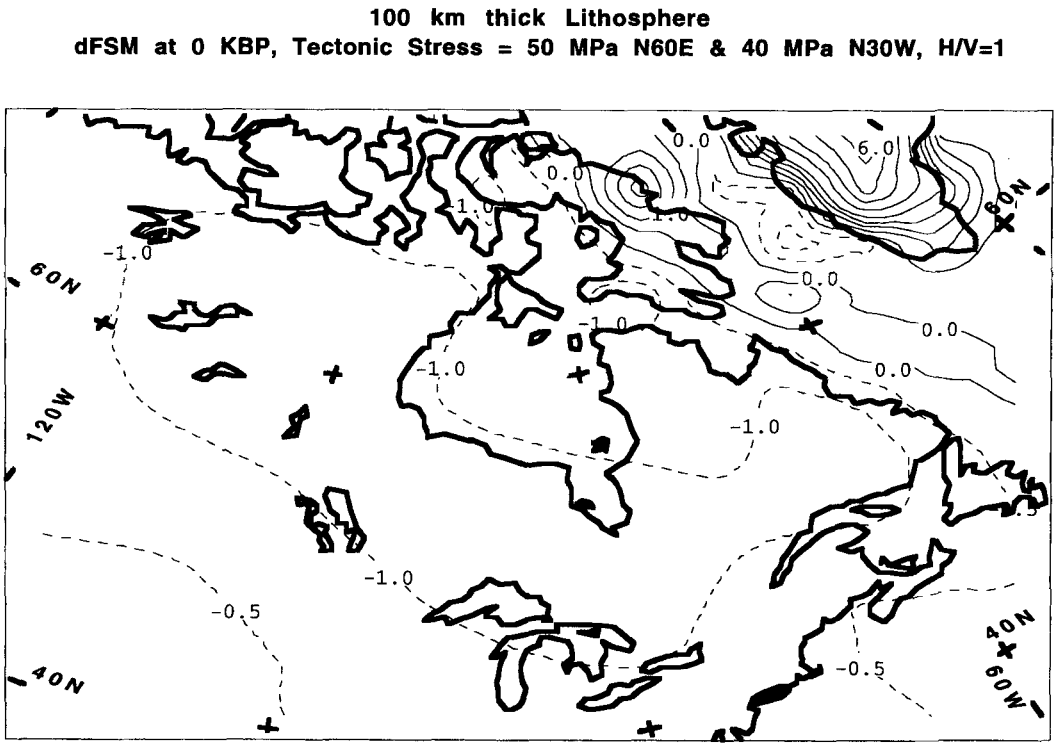

Figure 11. Similar to Fig. 3, except that a 100 km thick lithosphere is used in the model.

the peripheral area during the last 5,000 years; and (2) normal faulting is promoted during the loading phase for sites near and beyond the edge of the ice sheet. Again, these results are in agreement with those predicted by the disc model (companion paper).

3.2 Effect of tectonic stress magnitude

To investigate the effect of tectonic stress on dFSM, different combinations of tectonic stress magnitudes have been tested. The perturbation is small inside the ice margin provided the tectonic stress magnitudes are greater than about 20 MPa. Since tectonic stress magnitudes in eastern Canada are likely to be much higher than 20 MPa (Hasegawa *et al.* 1985), such low magnitudes will not be considered. Thus, in Figs 9 and 10, the maximum tectonic principal stress is 800 MPa and the minimum tectonic principal stress is 500 MPa (Zoback *et al.* 1994). Comparison of Figs 3(d) and 4 with Figs 9 and 10 shows that changes in the values of dFSM are generally insignificant. The only exceptions are for sites near the edge of the margin along the Labrador and US east coasts, where the value of dFSM increases slightly so that the onset of instability is delayed.

3.3 Effects of lithospheric properties

In Sections 3.1 and 3.2, the elastic lithosphere is set at 200 km thick (Peltier 1985). In this subsection we investigate the effect of a 100 km thick lithosphere. A comparison of Figs 11 and 12 with Figs 3(d) and 4 indicates that lithospheric thickness affects the magnitude of dFSM by only a small amount; consequently, only the timing of the onset of instability near the ice margin is delayed.

Effects of mantle viscosity and the ductile lower crust within an elastic lithosphere (Rydelek & Pollitz 1994) will be presented in a future paper.

4 SUMMARY AND DISCUSSION

Through the use of a realistic ice model (ICE-3G model of Tushingham & Peltier 1991) in conjunction with an earth model that predicts rebound rates compatible with observations, we have derived the following results.

(1) Under a wide range of tectonic stress magnitudes and values of the overburden stress parameter, ζ, crustal loading promotes fault stability directly under the load, in agreement with Johnston (1987, 1989).

(2) Within the ice margin, dFSM (for values of ζ close to unity) becomes negative and attains a minimum value soon after deglaciation is complete. This observation implies that postglacial faulting should be at its maximum at this time. This prediction is in agreement with available data in eastern Canada (Adams 1989; Shilts *et al.* 1992), as well as extensive observations of postglacial faulting in Fennoscandia (Mörner 1978; Lagerback 1979; Henkel 1978; Lagerback & Witschard 1983).

(3) Along the peripheral bulge in the northeastern United States, dFSM values (for ζ close to unity) indicate a transition from a stable to an unstable stress environment at a time that coincides with the occurrence of a significant prehistoric earthquake (Obermeier *et al.* 1991). Thrust faulting is manifest in several regions of northeastern United States; an example is the M_W5.4 southern Illinois earthquake of November 1968 (Herrmann 1979). Thus the analysis in this study can account for the thrust faults in the peripheral bulge in northeastern United States, but not the strike-slip faults (in agreement with James & Bent 1994).

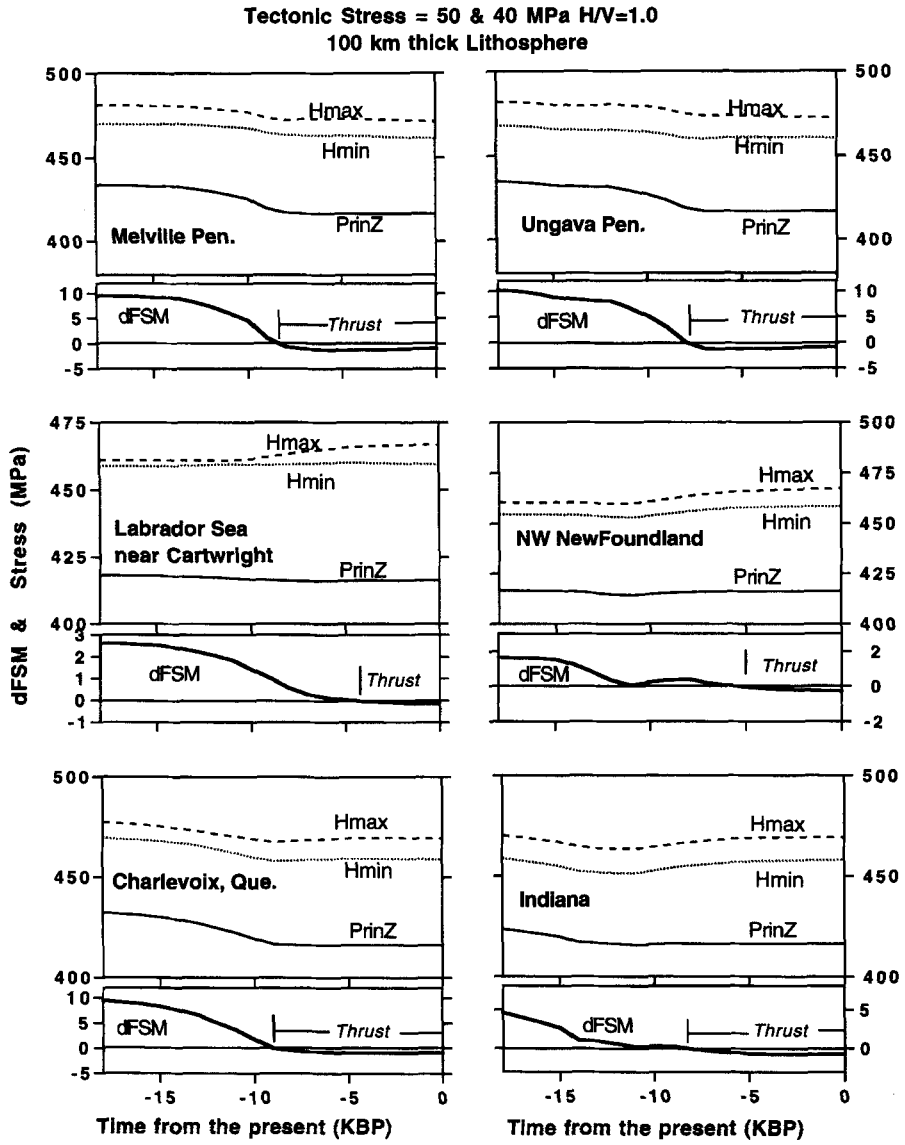

Figure 12. Similar to Fig. 4, except that a 100 km thick lithosphere is used in the model.

(4) The observation that (for ζ close to unity), the model does not predict drastic changes in dFSM (since deglacial time) along the seismotectonic trends shown in Fig. 1 implies that tectonic processes are controlling seismic activity along these trends at present (Adams & Basham 1989). Thus, at most, rebound stresses can act as a trigger mechanism for faults that are otherwise close to failure (*cf.* Quinlan 1984). This may be one of the factors contributing to the discrepancy between rebound strain rates and seismic strain rates along the St. Lawrence Valley as calculated by James & Bent (1994).

(5) Along the northeast coast of Baffin Island, an enhanced gradient in dFSM (Fig. 7b) is compatible with the steep gradients in postglacial uplift contours that are averages over the past 8000 years (*cf.* Basham *et al.* 1977).

(6) Stress measurements (Adams & Bell 1991) indicate that for most parts of the Canadian Shield and the St. Lawrence Platform, the vertical stress is the minimum principal stress at seismogenic depths, thus the results for $\zeta \geq 1$ (Figs 3 & 4) apply. However, in the Western Canadian Basin, the vertical stress is usually the intermediate principal stress, thus the results for $\zeta = 0.9$ (Figs 5 & 6) apply. This may also explain why Western Canada east of the Rocky Mountains is relatively aseismic at present (Fig. 5b). Future stress measurements along Baffin Island and along the Labrador coast may help to understand the causes of seismicity there.

In conclusion, the application of a realistic ice loading–unloading history, *vis-à-vis* the simple disc load in the companion paper, predicts the spatio–temporal pattern of fault instability and earthquake failure modes compatible with the companion paper, but more in accord with actual data.

ACKNOWLEDGMENTS

This work was supported by a grant to PW from NSERC of Canada. We thank Drs Arch Johnston and Thomas James for their useful suggestions, and Dr Doug Phillips for computer support.

REFERENCES

Adams, J., 1989. Postglacial faulting in eastern Canada: nature, origin and seismic hazard implications, *Tectonophysics,* **163,** 323–331.

Adams, J., 1996. Paleoseismology in Canada: A dozen years of progress, *J. geophys. Res.,* **101,** 6193–6207.

Adams, J. & Basham, P.W., 1989. The seismicity and seismotectonics of Canada east of the Cordillera, *Geosci. Canada,* **16,** 3–16.

Adams, J. & Bell, J.S., 1991. Crustal stresses in Canada, in *The Geology of North America,* Decade Map Vol. 1, *Neotectonics of North America,* pp. 367–386, eds. Slemmons, D.B., Engdahl, E.R., Zoback, M.D. & Blackwell, D.D., Geological Society of America, Boulder, CO.

Amelung, F. & Wolf, D., 1994. Viscoelastic perturbations of the earth: significance of the incremental gravitational force in models of glacial isostasy, *Geophys. J. Int.,* **117,** 864–879.

Basham, P.W., Forsyth, D.A. & Wetmiller, R.J., 1977. The seismicity of northern Canada, *Can. J. Earth Sci.,* **14,** 1646–1667.

Cathles, L.M., 1975. *The Viscosity of the Earth's Mantle,* Princeton University Press, Princeton, NJ.

Farrell, W.E. & Clark, J.A., 1976. On postglacial sea level, *Geophys. J. R. astr. Soc.,* **46,** 647–667.

Hasegawa, H.S. & Adams, J., 1990. Reanalysis of the 1963 Baffin Island earthquake (Ms 6.2) and its seismotectonic environment, *Seism. Res. Lett.,* **61,** 181–192.

Hasegawa, H.S. & Basham, P.W., 1989. Spatial correlation between seismicity and postglacial rebound in Eastern Canada, in *Earthquakes at North-Atlantic Passive Margins: Neotectonics and Postglacial Rebound,* pp. 483–500, eds Gregersen, S. & Basham, P.W., Kluwer, Dordrecht.

Hasegawa, H.S., Adams, J. & Yamazaki, K., 1985. Upper crustal stresses and vertical stress migration in eastern Canada. *J. geophys. Res.,* **90,** 3637–3648.

Henkel, H., 1978. Dislocation sets in northern Sweden, *Geol. Foren. Stockh. Forth.,* **100,** 271–278.

Herrmann, R.B., 1979. Surface wave focal mechanisms for eastern North American earthquakes with tectonic implications, *J. geophys. Res.,* **84,** 3543–3552.

James, T.S. & Bent, A.L., 1994. A comparison of eastern North American seismic strain-rates to glacial rebound strain-rates, *Geophys. Res. Lett.,* **21,** 2127–2130.

Johnston, A.C., 1987. Suppression of earthquakes by large continental ice sheets, *Nature,* **330,** 467–469.

Johnston, A.C., 1989. The effect of large ice sheets on earthquake genesis, in *Earthquakes at North-Atlantic Passive Margins: Neotectonics and Postglacial Rebound,* pp. 581–599, eds. Gregersen, S. & Basham, P.W., Kluwer, Dordrecht.

Lagerback, R., 1979. Neotectonic structures in northern Sweden, *Geol. Foren. Stockh. Forh.,* **100,** 263–269.

Lagerback, R. & Witschard, F., 1983. Neotectonics in northern Sweden—geological investigations, *Geol. Ser. Sweden, Tech. Rept,* **83–58,** 1–58.

Mitrovica, J.X. & Peltier, W.R., 1991. On post-glacial geoid relaxation over the equatorial oceans, *J. geophys. Res.,* **96,** 20 053–20 071.

Mörner, N.A., 1978. Faulting, fracturing and seismicity as functions of glacio-isostasy in Fennoscandia, *Geology,* **6,** 41–45.

Nabelek, J. & Suarez, G., 1989. The 1983 Goodnow earthquake in Central Adirondacks, New York: rupture of a simple, circular crack, *Bull. seism. Soc. Am.,* **79,** 1762–1777.

Obermeier, S.F. *et al.* 1991. Evidence of strong earthquake shaking in the lower Wabash Valley from prehistoric liquefaction features, *Science,* **251,** 1061–1063.

Peltier, W.R., 1985. The thickness of the continental lithosphere, *J. geophys. Res.,* **89,** 11 303–11 316.

Peltier, W.R., Farrell, W.E. & Clark, J.A., 1978. Glacial isostasy and relative sea level: a global finite element model, *Tectonophysics,* **50,** 81–110.

Quinlan, G., 1984. Postglacial rebound and the focal mechanisms of eastern Canadian earthquakes, *Can. J. Earth Sci.,* **21,** 1018–1023.

Rydelek, P.A. & Pollitz, F.F., 1994. Fossil strain from the 1811–1812 New Madrid earthquakes, *Geophys. Res. Lett.,* **21,** 2303–2306.

Shilts, W.W., Rappol, M. & Blais, A., 1992. Evidence of late and postglacial seismic activity in the Temiscouata–Madawaska Valley, Quebec–New Brunswick, Canada, *Can. J. Earth Sci.,* **29,** 1043–1059.

Stein, S., Sleep, N.H., Geller, R.J., Wang, S.C. & Kroeger, G.C., 1979. Earthquakes along the passive margin of Eastern Canada, *Geophys. Res. Lett.,* **6,** 537–540.

Talwani, P. & Rajendran, K., 1991. Some seismological and geometric features of intraplate earthquakes, *Tectonophysics,* **186,** 19–41.

Tushingham, A.M. & Peltier, W.R., 1991. Ice-3G: a new global model of late Pleistocene deglaciation based upon geophysical predictions of post-glacial relative sea level change. *J. geophys. Res.,* **96,** 4497–4523.

Tushingham, A.M. & Peltier, W.R., 1992. Validation of the ICE-3G model of Wurm–Wisconsin deglaciation using a global data base of relative sea level histories, *J. geophys. Res.,* **97,** 3285–3304.

Walcott, R.I., 1970. Isostatic response to loading of the crust in Canada, *Can. J. Earth Sci.,* **7,** 716–727.

Wu, P., 1992. Deformation of an incompressible viscoelastic flat earth with power law creep: a finite element approach, *Geophys. J. Int.,* **108,** 136–142.

Wu, P., 1993. Post-glacial rebound in a power-law medium with axial symmetry and the existence of the transition zone in relative sea level data, *Geophys. J. Int.,* **114,** 417–432.

Wu, P., 1996. Changes in orientation of near-surface stress field as constraints to lower-mantle viscosity and horizontal principal tectonic stress difference in Eastern Canada, *Geophys. Res. Lett.,* in press.

Wu, P. & Hasegawa, H., 1996. Induced stresses and fault potential in eastern Canada due to a disc load: a preliminary analysis, *Geophys. J. Int.,* **125,** 415–430.

Wu, P. & Peltier, W.R., 1982. Viscous gravitational relaxation, *Geophys. J. R. astr. Soc.,* **70,** 435–486.

Wu, P. & Peltier, W.R., 1983. Glacial isostatic adjustment and the free air gravity anomaly as a constraint on deep mantle viscosity, *Geophys. J. R. astr. Soc.,* **74,** 377–450.

Zoback, M.L., 1992. Stress field constraints on intraplate seismicity in eastern North America, *J. geophys. Res.,* **97,** 11 761–11 782.

Zoback, M.D. *et al.* 1994. Upper crustal strength inferred from stress measurements to 6 km depth in the KTB borehole, *Nature,* **365,** 633–635.